Fermi National Accelerator Laboratory

The CDF Detector: An Overview[*]

F. Abe[p], D. Amidei[c], G. Apollinari[k], G. Ascoli[g], M. Atac[d], P. Auchincloss[n], A.R. Baden[f], A. Barbaro-Galtieri[i],
V. E. Barnes[l], E. Barsotti[d], F. Bedeschi[k], S. Belforte[k], G. Bellettini[k], J. Bellinger[q], J. Bensinger[b], A. Beretvas[n],
P. Berge[d], S. Bertolucci[e], S. Bhadra[g], M. Binkley[d], R. Blair[a], C. Blocker[b], J. Bofill[d], A.W. Booth[d], G. Brandenburg[f],
A. Brenner[d], D. Brown[f], A. Byon[l], K.L. Byrum[q], M. Campbell[c], R. Carey[f], W. Carithers[i], D. Carlsmith[q],
J.T. Carroll[d], R. Cashmore[1], F. Cervelli[k], K. Chadwick[l], T. Chapin[m], G. Chiarelli[k], W. Chinowsky[i], S. Cihangir[o],
D. Connor[j], M. Contreras[b], J. Cooper[d], M. Cordelli[e], M. Curatolo[e], C. Day[d], R. DelFabbro[k], M. Dell'Orso[k],
L. DeMortier[b], T. Devlin[n], D. DiBitonto[o], R. Diebold[a], F. Dittus[d], A. DiVirgilio[k], R. Downing[g], G. Drake[d],
T. Droege[d], M. Eaton[f], J. Elias[d], R. Ely[i], S. Errede[g], B. Esposito[e], A. Feldman[f], B. Flaugher[n], E. Focardi[k],
G.W. Foster[d], M. Franklin[f,g], J. Freeman[d], H. Frisch[c], Y. Fukui[h], I. Gaines[d], A.F. Garfinkel[l], P. Giannetti[k],
N. Giokaris[m], P. Giromini[e], L. Gladney[j], M. Gold[i], K. Goulianos[m], J. Grimson[d], C. Grosso-Pilcher[c], C. Haber[i],
S. Hahn[j], R. Handler[q], D. Hanssen[d], R.M. Harris[i], J. Hauser[c], Y. Hayashide[p], T. Hessing[o], R. Hollebeek[j],
L. Holloway[g], P. Hu[n], B. Hubbard[i], P. Hurst[g], J. Huth[d], M. Ito[p], J. Jaske[q], H. Jensen[d], R.P. Johnson[d], U. Joshi[n],
R.W. Kadel[d], T. Kamon[o], S. Kanda[p], I. Karliner[g], H. Kautzky[d], K. Kazlauskis[n], E. Kearns[f], R. Kephart[d], P. Kesten[b],
H. Keutelian[g], Y. Kikuchi[p], S. Kim[p], L. Kirsch[b], S. Kobayashi[2], K. Kondo[p], U. Kruse[g], S. Kuhlmann[i],
A.T. Laasanen[l], W. Li[a], T. Liss[c], N. Lockyer[j], F. Marchetto[o], R. Markeloff[q], L.A. Markosky[q], M. Masuzawa[p],
P. McIntyre[o], A. Menzione[k], T. Meyer[o], S. Mikamo[h], M. Miller[j], T. Mimashi[p], S. Miscetti[e], M. Mishina[h],
S. Miyashita[p], H. Miyata[p], N. Mondal[q], S. Mori[p], Y. Morita[p], A. Mukherjee[d], A. Murakami[2], Y. Muraki[3],
C. Nelson[d], C. Newman-Holmes[d], L. Nodulman[a], J. O'Meara[d], G. Ott[q], T. Ozaki[p], S. Palanque[4], R. Paoletti[k],
A. Para[d], J. Patrick[d], R. Perchonok[d], T.J. Phillips[f], H. Piekarz[b], R. Plunkett[m], L. Pondrom[q], J. Proudfoot[a], G. Punzi[k],
D. Quarrie[d], K. Ragan[j], G. Redlinger[c], R. Rezmer[a], J. Rhoades[q], L. Ristori[k], T. Rohaly[j], A. Roodman[c], H. Sanders[c],
A. Sansoni[e], R. Sard[g], V. Scarpine[g], P. Schlabach[g], E.E. Schmidt[d], P. Schoessow[a], M. H. Schub[l], R. Schwitters[f],
A. Scribano[k], S. Segler[d], M. Sekiguchi[p], P. Sestini[k], M. Shapiro[f], M. Sheaff[q], M. Shibata[p], M. Shochet[c], J. Siegrist[i],
V. Simaitis[g], J. K. Simmons[l], P. Sinervo[d], M. Sivertz[5], J. Skarha[q], D.A. Smith[g], R. Snider[c], L. Spencer[b],
R. St.Denis[f], A. Stefanini[k], Y. Takaiwa[p], K. Takikawa[p], S. Tarem[b], D. Theriot[d], J. Ting[c], A. Tollestrup[d], G. Tonelli[k],
W. Trischuk[f], Y. Tsay[c], K. Turner[d], F. Ukegawa[p], D. Underwood[a], C. vanIngen[d], R. VanBerg[j], R. Vidal[d],
R.G. Wagner[a], R.L. Wagner[d], J. Walsh[j], T. Watts[n], R. Webb[o], T. Westhusing[g], S. White[m], V. White[d], A. Wicklund[a],
H.H. Williams[j], T. Winch[q], R. Yamada[d], T. Yamanouchi[d], A. Yamashita[p], K. Yasuoka[p], G.P. Yeh[d], J. Yoh[d], F. Zetti[k]

CDF Member Institutions

[a] Argonne National Laboratory - [b] Brandeis University - [c] University of Chicago - [d] Fermi National Accelerator
Laboratory - [e] INFN, Laboratori Nazionali di Frascati, Italy - [f] Harvard University - [g] University of Illinois -
[h] KEK, Japan - [i] Lawrence Berkeley Laboratory - [j] University of Pennsylvania - [k] INFN, University and Scuola
Narmale Superiore of Pisa, Italy - [l] Purdue University - [m] Rockefeller University - [n] Rutgers University -
[o] Texas A&M University - [p] University of Tsukuba, Japan - [q] University of Wisconsin

Visitors

[1] Oxford University, England - [2] Saga University, Japan - [3] ICRR, Tokyo University, Japan -
[4] CEN, Saclay, France - [5] Haverford College, Haverford, PA.

February 5, 1988

The CDF Detector: An Overview

F.Abe[p], D.Amidei[c], G.Apollinari[k], G.Ascoli[g], M.Atac[d], P.Auchincloss[n], A.R.Baden[f],
A. Barbaro-Galtieri[i], V.E.Barnes[l], E.Barsotti[d], F.Bedeschi[k], S.Belforte[k],
G.Bellettini[k], J.Bellinger[q], J.Bensinger[b], A.Beretvas[n], P.Berge[d], S.Bertolucci[e],
S.Bhadra[g], M.Binkley[d], R.Blair[a], C.Blocker[b], J.Bofill[d], A.W.Booth[d], G.Brandenburg[f],
A.Brenner[d], D.Brown[f], A.Byon[l], K.L.Byrum[q], M.Campbell[c], R.Carey[f], W.Carithers[i],
D.Carlsmith[q], J.T.Carroll[d], R.Cashmore[1], F.Cervelli[k], K.Chadwick[i], T.Chapin[m],
G.Chiarelli[k], W.Chinowsky[i], S.Cihangir[o], D.Connor[j], M. Contreras[b], J.Cooper[d],
M.Cordelli[e], M.Curatolo[e], C.Day[d], R.DelFabbro[k], M.Dell'Orso[k], L.DeMortier[b],
T.Devlin[n], D.DiBitonto[o], R.Diebold[a], F.Dittus[d], A.DiVirgilio[k], R.Downing[g], G. Drake[d],
T.Droege[d], M.Eaton[f], J.E.Elias[d], R.Ely[i], S.Errede[g], B.Esposito[e], A.Feldman[f], B.Flaugher[n],
E.Focardi[k], G.W.Foster[d], M.Franklin[f,g], J.Freeman[d], H.Frisch[c], Y.Fukui[h], I.Gaines[d], A.F.Garfinkel[l],
P.Giannetti [k], N.Giokaris[m], P.Giromini[e], L.Gladney[j], M.Gold[i], K.Goulianos[m], J.Grimson[d],
C.Grosso-Pilcher[c], C.Haber[i], S.R.Hahn[j], R.Handler[q], D.Hanssen[d], R.M.Harris[i], J.Hauser[c],
Y.Hayashide[p]. T.Hessing[o], R.Hollebeek[j], L.Holloway[g], P.Hu[n], B.Hubbard[i], P.Hurst[g], J.Huth[d],
M.Ito[p], J.Jaske[q], H.Jensen[d], R.P.Johnson[d], U.Joshi[n], R.W.Kadel[d], T.Kamon[o], S.Kanda[p],
I.Karliner[g], H.Kautzky[d], K.Kazlauskis[n], E.Kearns[f], R.Kephart[d], P.Kesten[b], H.Keutelian[g],
Y.Kikuchi[p], S.Kim[p], L.Kirsch[b], S.Kobayashi[2], K.Kondo[p], U.Kruse[g], S.E.Kuhlmann[i], A.T.Laasanen[l],
W.Li[e], T.Liss[c], N.Lockyer[j], F.Marchetto[o], R.Markeloff[q], L.A. Markosky[q], M.Masuzawa[p],
P.McIntyre[o], A.Menzione[k], T.Meyer[o], S.Mikamo[h], M.Miller[j], T.Mimashi[p], S.Miscetti[e],
M.Mishina[h], S.Miyashita[p], H.Miyata[p], N.Mondal[q], S.Mori[p], Y.Morita[p], A.Mukherjee[d],
A.Murakami[2], Y.Muraki[3], C.Nelson[d], C.Newman-Holmes[d], L.Nodulman[a], J.O'Meara[d],
G.Ott[q], T.Ozaki[p], S.Palanque[4], R.Paoletti[k], A.Para[d], J.Patrick[d], R.Perchonok[d], T.J.Phillips[f],
H.Piekarz[b], R.Plunkett[m], L.Pondrom[q], J.Proudfoot[a], G.Punzi[k], D.Quarrie[d], K.Ragan[j], G.Redlinger[c],
R.Rezmer[a], J.Rhoades[q], L.Ristori[k], T.Rohaly[j], A.Roodman[c], H.Sanders[c],
A.Sansoni[e], R.Sard[g], V.Scarpine[g], P.Schlabach[g], E.E.Schmidt[d], P.Schoessow[a],
M.H.Schub[l], R.Schwitters[f], A.Scribano[k], S.Segler[d], M.Sekiguchi[p], P.Sestini[k], M.Shapiro[f],
M.Sheaff[q], M.Shibata[p], M.Shochet[c], J.Siegrist[i], V.Simaitis[g], J.K.Simmons[i], P.Sinervo[j],
M.Sivertz[b], J.Skarha[q], D.A.Smith[g], R.Snider[c], L.Spencer[b], R.St.Denis[f], A.Stefanini[k],
Y.Takaiwa[p], K.Takikawa[p], S.Tarem[b], D.Theriot[d], J.Ting[c], A.Tollestrup[d], G.Tonelli[k],
W.Trischuk[f], Y.Tsay[c], K.Turner[d], F.Ukegawa[p], D.Underwood[a], C.vanIngen[d], R.VanBerg[j],
R.Vidal[d], R.G.Wagner[a], R.L.Wagner[d], J.Walsh[j], T.Watts[n], R.Webb[o], T.Westhusing[g],
S.White[m], V.White[d], A.Wicklund[a], H.H.Williams[j], T.Winch[q], R.Yamada[d],
T.Yamanouchi[d], A.Yamashita[p], K.Yasuoka[p], G.P.Yeh[d], J.Yoh[d], F.Zetti[k]

CDF Member Institutions

[a] Argonne National Laboratory- [b] Brandeis University- [c] University of Chicago
[d] Fermi National Accelerator Laboratory- [e] INFN, Laboratori Nazionali di Frascati, Italy
[f] Harvard University- [g] University of Illinois- [h] KEK, Japan
[i] Lawrence Berkeley Laboratory-[j] University of Pennsylvania
[k] INFN, University and Scuola Normale Superiore of Pisa, Italy- [l] Purdue University
[m] Rockefeller University- [n] Rutgers University- [o] Texas A&M University
[p] University of Tsukuba, Japan- [q] University of Wisconsin

Visitors

[1] Oxford University, England- [2] Saga University, Japan
[3] ICRR, Tokyo University, Japan- [4] CEN, Saclay, France-
[5] Haverford College, Haverford, PA.

Abstract

The Collider Detector at Fermilab (CDF) is a 5000 ton magnetic detector built to study 2 TeV $\bar{p}p$ collisions at the Fermilab Tevatron. Event analysis is based on charged particle tracking, magnetic momentum analysis and fine-grained calorimetry. The combined electromagnetic and hadron calorimetry has approximately uniform granularity in rapidity-azimuthal angle and extends down to 2 degrees from the beam direction. Various tracking chambers cover the calorimeter acceptance and extend charged particle tracking down to 2 mrad from the beam direction. Charged particle momenta are analyzed in a 1.5 T solenoidal magnetic field, generated by a superconducting coil which is 3 m in diameter and 5 m in length. The central tracking chamber measures particle momenta with a resolution better than $\delta p_T/p_T^2 = 2 \times 10^{-3}$ $(GeV/c)^{-1}$ in the region $40° < \theta < 140°$ and $\delta P_T/p_T^2 \leq 4 \times 10^{-3}$ for $21° < \theta < 40°$ and $140° < \theta < 159°$. The calorimetry, which has polar angle coverage from 2° to 178° and full azimuthal coverage, consists of electromagnetic shower counters and hadron calorimeters, and is segmented into about 5000 projective "towers" or solid angle elements. Muon coverage is provided by drift chambers in the region $56° < \theta < 124°$, and by large forward toroid systems in the range $3° < \theta < 16°$ and $164° < \theta < 177°$. Isolated high momentum muons can be identified in the intermediate angular range by a comparison of the tracking and calorimeter information in many cases. A custom front-end electronics system followed by a large Fastbus network provides the readout of the approximately 100,000 detector channels. Fast Level 1 and Level 2 triggers make a detailed pre-analysis of calorimetry and tracking information; a Level 3 system of on-line processors will do parallel processing of events. This paper provides a summary of the aspects of the detector which are relevant to its physics capabilities, with references to more detailed descriptions of the subsystems.

A. Introduction

The Fermilab Tevatron collider is currently the world's highest energy accelerator, colliding anti-protons with protons at a center-of-mass energy of 1.8 TeV. The Collider Detector at Fermilab (CDF), is the first general purpose detector built to exploit this machine. The partially completed apparatus detected the first $\bar{p}p$ collisions at the Tevatron in October, 1985. The first physics run, from January 1987 to May 1987, was with an essentially complete detector. Analysis of these data is now in full swing.

The individual sub-systems of the detector have been described in a series of detailed papers.[1] Here we give an overview of these systems, with particular emphasis on details such as geometrical coverage which have a direct bearing on physics results, and provide in one place a list of references for those interested in the technical details.

B. Overall Layout

The detector consists of a 2000 ton moveable central detector which is made up of the solenoidal magnet, steel yoke, tracking chambers, electromagnetic shower counters, hadron calorimeters and muon chambers, and two identical forward/backward detectors consisting of segmented time-of-flight counters, electromagnetic shower counters, hadron calorimeters, and muon toroidal spectrometers. A perspective view is shown in Figure 1. A photograph of the central detector alone is shown in Figure 2. The steel yoke forms a large "box" 9.4 m high by 7.6 m wide by 7.3 m long. The 3 m diameter, 5 m long superconducting coil and the calorimeterized end-plugs are supported by the yoke. The central calorimeter consists of 48 wedge-shaped modules assembled into four self-supporting arches which rest on the yoke base. The arches can be retracted to service the modules (Figure 3). The whole yoke assembly, with the arches resting on it, rolls from its garaged position in the CDF assembly building to its position on the Tevatron beam line (Figure 4). The cables follow it on an overhead flexible cable tray. The 31.4 m move takes one day.

An elevation view of the forward half of the complete detector is shown in Figure 5. The detector is divided into a central detector ($10° < \theta < 170°$), which includes the end-plugs which form the pole pieces for the solenoidal magnet ($10° < \theta_s < 30°$), and the forward/backward regions ($\theta_s < 10°$), where θ_s is the polar angle measured from either the proton or antiproton beam. At angles less than 10° to either beam, particles produced at the interaction point exit the conical hole in the end plug and strike the forward shower counters and hadron

calorimeters. On each end the calorimeters are followed by two 7.6 m-diameter steel toroidal magnets used as muon spectrometers. A forward muon spectrometer and forward calorimeters are shown in Figure 6. Single planes of scintillation counters at the face of the forward shower counter on each end provide a "minimum bias" trigger and luminosity monitor.

C. Detector Components

The basic goal for CDF is to measure the energy, momentum, and, where possible, the identity, of particles produced at the Tevatron collider over as large a fraction of the solid angle as practical. Our strategy to accomplish this was to surround the interaction region with layers of different detector components. Starting at the interaction point, particles encounter in sequence: a thin wall Be vacuum chamber, charged particle tracking chambers, sampling calorimeters, and muon detectors. Because the "natural" phase space for energetic hadron collisions is described by rapidity, transverse momentum, and azimuthal angle, we have chosen an approximately cylindrically symmetric layout of detector components with segmentation roughly uniform in pseudo-rapidity (η) and azimuth (ϕ).[2]

Brief descriptions of the detector components follow in order of location from the interaction point.

Tracking

There are four separate tracking systems in the CDF detector (see Fig. 5). In this section, the tracking systems that overlap the calorimeter acceptance (angles greater than 2 degrees with respect to the beam direction) are described. Using special vacuum chamber insertions, the tracking extends to smaller angles. This very small angle system is described below.

Immediately outside the vacuum chamber, eight small vertex time projection chambers (the VTPC system)[3] track charged particles at angles greater than 3.5° from the beam line, and give good pointing in the θ direction. The forward tracking system (FTC)[4] allows reconstruction of tracks which exit the central detector through the 10° hole in the end plugs and which then strike the forward shower counters and calorimeters. The Central Tracking Chamber (CTC)[5] is a large cylindrical drift chamber with excellent spatial and momentum resolution used to measure charged tracks in the central region. A system of central drift tubes (the CDT system)[6] with high resolution charge division surrounding the CTC provide a correlated R-ϕ-Z measurement. The physical parameters of these four tracking systems are listed in Table 1. The momentum resolution for charged tracks versus polar angle is given in Table 2.

The VTPC system comprises eight separate time projection chamber modules which are mounted end-to-end along the beam direction. The 2.8 meter total length of the chamber covers well the long interaction region ($\sigma_z \sim 35$ cm). The VTPC chambers contain a total of 3072 sense wires for the measurement of track coordinates in R-Z, where R is the radial distance from the beam and Z is the distance along the beam line from the center of the detector, and 3072 pads for the measurement of coordinates in R-ϕ. Figure 7 is a schematic drawing of two octagonal VTPC modules. Each module has a central high voltage grid that divides it into two 15 cm-long drift regions. At the end of each drift region there are proportional chambers arranged in octants, each octant with 24 anode sense wires and 24 cathode pads. As viewed from the drift region, an octant consists of a cathode grid (screen) followed by a plane of field shaping wires, a plane of sense wires which alternate in the radial direction with the field wires, and a resistive cathode plane. Three rows of pads are located behind the resistive cathode. The active area of the chamber extends from R = 6.8 cm to R = 21 cm.

Since particles detected by the calorimeters and other tracking chambers first pass through the VTPC, a considerable effort was made to minimize the mass of the VTPC and the beam pipe. The beam pipe, inside the VTPC, consists of a 5.08 cm diameter Be tube, with a wall thickness of 500 μm. Figure 8 shows a detail of the region surrounding the beam pipe. Figure 9 is a plot of the amount of material in radiation lengths versus the polar angle as measured from the interaction point.

The forward tracking chamber (FTC) is a radial drift chamber which, in conjunction with the VTPC, is responsible for tracking in the angular region $2° < \theta_s < 10°$. The 72 wedge shaped cells of an FTC are shown schematically in Figure 10. The chamber contains planes of radial anode and field shaping wires which alternate with planes of cathode strips. The planes are slanted by 2° relative to the beam axis so that left-right ambiguities can be resolved by demanding that tracks point back to the vertex. Each anode plane has twenty-one sense wires and twenty-six field shaping wires. Four of the twenty-one sense wires are instrumented for charge division, so that an R-ϕ-Z measurement can be made for each track.

The Central Tracking Chamber (CTC) is a 1.3 m radius 3.2 m long cylindrical drift chamber which gives precise momentum measurements in the angular region $40° < \theta < 140°$ (-1 < η < 1). In this region the momentum resolution is better than $\delta p_T / p_T^2 \leq .002$ (GeV/c)$^{-1}$. The chamber contains 84 layers of sense wires grouped into 9 "superlayers." Five of the superlayers consist

of 12 axial sense wires; four stereo superlayers consist of 6 sense wires tilted by ±3° relative to the beam direction. Figure 11 shows an endplate of the chamber displaying the 45° tilt of the superlayers to the radial direction to correct for the Lorentz angle of the electron drift in the magnetic field.

The CDT system consists of three layers of 3 m long, 1.27 cm diameter stainless steel tubes mounted on the outer perimeter of the CTC. A correlated R-ϕ-Z determination (i.e. a space point) is made by making both drift-time and charge division measurements. Typical resolutions are 2.5 mm in the axial (beam) direction and 200 μm in the azimuthal direction. Figure 12 shows a cross section of a small region of the CDT system.

Solenoid Magnet Coil

Precise momentum determination for charged particles produced in the central region is provided by the CTC, which is in a uniform 1.5 T magnetic field oriented along the incident beam direction. The field is produced by a 3 m diameter 5 m long superconducting solenoidal coil.[7] The coil is made of 1164 turns of an aluminum-stabilized NbTi/Cu superconductor, fabricated by the EFT method (extrusion with front tension) in which high purity aluminum is friction welded to the superconducting wire during the extrusion process.[8] The coil was designed to have no inner bobbin: the radially outward magnetic forces are supported by a thin aluminum-alloy cylinder outside the coil. Cooling is by forced flow of two-phase helium through an aluminum tube welded to the outer support cylinder. The overall radial thickness of the solenoid is 0.85 radiation lengths.

Calorimeters

Because of the importance of hadronic jets in high energy proton-antiproton collisions, a "tower" geometry was chosen for all calorimeters. The coverage of the calorimeter towers in η-ϕ space[2] is shown in Figure 13. Each tower has an electromagnetic shower counter in front of a corresponding hadron calorimeter, so that one can make a detailed comparison of electromagnetic to hadronic energy on a tower-by-tower basis. The towers are projective, i.e., they point at the interaction region, and are 0.1 units of η wide by 15° (central region) or 5° (plug and forward regions) in ϕ. The physical size of a tower ranges from about 24.1 cm (η) × 46.2 cm (ϕ) in the central region to 1.8 cm × 1.8 cm in the forward region. A summary of the calorimeter properties in the different angular regions is given in Table 3.

The electromagnetic shower counters use lead sheets interspersed with scintillator as the active detector medium in the central region, and with

proportional chambers with cathode pad readout elsewhere. The electromagnetic shower counters have a spatial resolution of ~~2 mm over the complete solid angle. The depth segmentation for each tower of the central shower counter[9] (0 < $|\eta|$ < 1.1) consists of a single overall sample, with an additional measurement with high spatial resolution transverse to the shower using a proportional chamber located at a depth of 6 radiation lengths. In the end plug shower counters[10] (1.1 < $|\eta|$ < 2.4) there are 3 samples in depth, integrating over 3.8, 14.2, and 3.0 radiation lengths. Each wire plane in depth, 34 in number, is also digitized by quadrant, giving a detailed shower profile in addition to the three depth samples for isolated electrons or photons. The forward region shower counters[11] (2.2 < $|\eta|$ < 4.2) have two depth segments, each integrating over 12 radiation lengths. As in the plug, the wire planes at each depth are read out for profile information, but with five separate regions per quadrant.

The hadron calorimeters consist of steel plates alternated with active detectors: plastic scintillator in the central region, and gas proportional chambers in the plug and forward/backward regions. The hadronic calorimeters have a slightly different sharing of the rapidity coverage from the electromagnetic shower counters due to the geometry of the solenoid. The calorimeters in the central detector[12] consist of the hadronic towers in the wedges, and also additional towers in the "endwalls," which are attached to the yoke (see Figure 5). The rapidity coverage of the central towers is 0 < $|\eta|$ < 1.3. The end plug hadron calorimeters[13] cover the region 1.3 < $|\eta|$ < 2.4, while the forward calorimeters[14] cover 2.3 < $|\eta|$ < 4.2. All the hadron calorimeters have only one depth sample, although the plug and forward calorimeters have the wires of each wire plane per quadrant digitized individually to provide shower profile information.

The calibration of each scintillator-based 'wedge' calorimeter was determined with 50 GeV electrons and charged pions in a test beam,[15] and with cosmic ray muons.[16] Long term gain variations are monitored by a set of ^{137}Cs sources, one per wedge, which can be moved through the module under remote control.[17] Short term gain changes are also monitored by light flasher systems.[17] The central EM calorimeters use a Xe lamp system connected by quartz fibers to the calorimeter, and also a light-emitting diode system connected by quartz fibers to a transition piece directly in front of each photomultiplier tube.[18] The hadron calorimeters employ a nitrogen laser, also connected by quartz fibers to the transition piece. Figure 14 shows the reproducibility of the calibration procedure for four wedges. Over a period of a few months, the procedure has an accuracy of better than 2%.

Changes in gain of the gas-based calorimeters due to variations in pressure, temperature or gas composition are tracked by calibrated monitor tubes. Gain changes of 25% over a 24 hour period have been recorded when a pressure front moves through the laboratory, but different monitor tubes show the same gain change to within about 2%. It appears that the ultimate precision with which the gas-based calorimeter gain changes can be tracked with the monitor tubes will be about 2%.

Muon Detection

There are two systems in CDF to measure muons which penetrate the calorimeters. In the central detector, each wedge contains 4 layers of muon chambers[19] at the end of the hadron calorimeter section. In both the forward and backward regions there is a muon spectrometer[20] consisting of large magnetized steel toroids with drift chamber planes and triggering scintillation counters. In the intervening intermediate region there is partial coverage for isolated muons. For example, the combination of the excellent momentum and spatial resolution of the central tracking chamber with the requirement of a minimum ionizing particle in the (finely-segmented) calorimeters allows finding the second muon in a Z^0 decay.

The layout of the central muon chambers is shown in Figure 15. The chambers measure four points along the trajectory with an accuracy of 250 μm per point in the ϕ direction (Fig. 16). Charge division gives an accuracy of $\sigma = 1.2$ mm per point in the Z direction. The chambers cover the angular region $56° < \theta < 124°$; in this region their average coverage is 84% due to the spaces between the chambers at the ϕ boundaries of the wedges and the boundary between the arches at $\theta = 90°$. The system is essentially 100% efficient for muons in its solid angle when the muon momentum is above 3 GeV/c. Muons are matched both in position and angle to tracks in the central tracking chamber (CTC). As with any high momentum track in the CTC, the momentum resolution on a central muon is better than $\delta p_T / p_T^2 < .002$ (GeV/c)$^{-1}$.

The layout of the forward/backward muon spectrometers is shown in Figure 5; an r-ϕ view is shown in Figure 17. Each spectrometer contains two 1 m thick, 7.82 m diameter, 395 ton steel toroids. The inner diameter is 0.914 m. Four coils excite the toroids to a magnetic field ranging from 2.0 T at the inner radius to 1.6 T at the outer radius. Three layers of electrodeless drift chambers measure the muon trajectory with an accuracy of 5° in the ϕ direction, and ~200 μ in the r direction. Two layers of scintillation counters provide trigger information. The angular region covered by each spectrometer lies between 3° and 16° from each

beam line. The momentum resolution is 13%, independent of momentum, for muons with total momentum P above 8 GeV (remember that $P_T = P\sin\theta$). Muons are matched to the FTC and VTPC tracking systems: isolated muons can also be matched to the calorimetry in front of the muon spectrometer.

Trigger Counters and Luminosity Monitoring

There is a plane of scintillation counters on the front face of each of the forward and the backward shower counters. These scintillators, called the beam-beam counters (BBC), provide a "minimum-bias" trigger for the detector, and are also used as the primary luminosity monitor. The counters have excellent timing properties ($\sigma < 200$ ps), and so provide the best measurement of the time of the interaction. A crude (± 4 cm) measurement of the vertex position is also obtained from the timing.

The counters are arranged in a rectangle around the beam pipe as shown in Figure 18. They cover the angular region (measured along either the horizontal or vertical axes) from 0.32° to 4.47°, corresponding to a pseudo-rapidity of range of 3.24 to 5.90. The minimum bias trigger requires at least one counter in each plane to fire within a 15 nsec window centered on the beam crossing time.

The Small Angle Silicon Detector and Chamber System

A system of seven stations of detectors (see Fig. 19) along the accelerator ring tracks particles produced at very small angles. Each of the outer stations, S_1, S_2, S_3, S_6 and S_7, consists of a pair of 'pots' which can be remotely moved to within a few mm of the beam. The two inner stations, S_4, and S_5, each have two pairs of pots separated by 1m which track particles in the angular region $2 < \theta_s < 6$ mrad, and drift chambers which cover the range $8 < \theta_s < 35$ mrad. Every pot contains two scintillation counters and a drift chamber with 4 sense wires and delay line readout. The stations also contain a single silicon detector with both horizontal and vertical strips, giving 50μ resolution in the horizontal plane and 300μ in the vertical. The subsystem S3-S6 covers the angular range $0.2 < \theta_s < 1.2$ mrad, corresponding to elastic scattering with momentum transfer $0.04 < |t| < 1.5$ (GeV/c)^2. Because the S1, S2, S3 spectrometer uses the Tevatron dipoles (and not just the low-β quadrupoles) the momentum resolution for 'leading particles' is good ($\Delta p/p \approx 0.1\%$ at p = 1000 GeV/c at all accessible angles and momentum transfers. In the proton direction momentum analysis is performed by the quadrupole field only, and the momentum resolution depends on angle (at $\theta = 1.0$ mrad, $\Delta p/p = 2\%$).

D.   Data Acquisition, Front-End Electronics and Readout

The CDF detector has a total of approximately 100,000 electronic channels consisting of photomultiplier tubes, strip/wire/pad chambers, drift chambers, drift chambers with current division readout, and silicon strip detectors. The calorimetry requires a very large dynamic range for the electronic readout, extending from a few tens of MeV to many hundreds of GeV. A special crate-based analog front-end system called the RABBIT System[21] was developed to deal with this problem. The RABBIT system consists of 129 crates mounted on the detector which service all of the calorimeters, about 60,000 channels of the 100,000 total. The drift chambers make up the bulk of the remainder: their signals are shaped at the detector and brought up from the collision hall to commercial Fastbus TDC modules in the counting room.

The measurement method upon which the RABBIT system is based involves sampling two voltage levels for each event to avoid pileup and common mode noise: one just before the interaction time to establish a reference level and another after the interaction. The difference between voltage levels is proportional to the integrated signal change. This approach makes use of the bunched structure of the beams. Normally, the Tevatron operates with three or six approximately equally spaced bunches of protons and antiprotons. Thus, interactions occur at relatively well defined "windows" in time, separated by 7 or 3.5 μsec. This general approach is referred to as "before-after" sampling. Digitization is performed in each crate.

As the RABBIT channels are digitized they are read out by fast intelligent scanners called MX's.[21] The scanners interface to the Fastbus data acquisition system.[22] Most of the tracking systems use commercial Fastbus modules which are read out by a second type of intelligent scanner called the SSP.[22] Each scanner can buffer four events, and handles approximately 1000 channels. There are approximately 60 MX scanners and 25 SSP scanners in the system.

The Fastbus network which comprises the Data Acquisition (DAQ) system consists of 53 crates, 16 cable segments, and 66 segment-interconnect modules. Many custom designed Fastbus modules, such as a hardware event builder, allow for the bandwidth necessary to transmit the data for each event. For a nominal event size of 100 Kbytes the DAQ system reads out events at 20-30 Hz into the Level 3 system (see below). A detailed technical description is given in reference 22.

E. Trigger System

Level 1 and Level 2

The trigger[23] is designed to exploit the projective geometry of the calorimeter towers. Both hadron and electromagnetic calorimeter towers are summed into trigger towers with a width in pseudo-rapidity of $\Delta\eta = 0.2$ and a width in ϕ of $\Delta\phi = 15°$. This results in a representation of the entire detector as a 42 (in η) by 24 (in ϕ) array for both the electromagnetic and hadronic calorimeters. Outputs from all phototubes are brought to the counting room individually and summed, four tubes per channel, into the $\Delta\phi = 15°$ and $\Delta\eta = 0.2$ trigger towers. All gas calorimeter pad signals are summed at the detector into the trigger towers. The signals are weighted by $\sin\theta$ to represent the "transverse energy," E_T, deposited in the tower.

The trigger signals from the calorimeters are sent to the trigger electronics on dedicated cables. The signals are DC levels (0-100 GeV in E_T is 0-1 volts) from the before-after sampling of the beam crossing. The voltage levels stay on these trigger cables until a Level 1 decision is made: if Level 1 is not satisfied in a given crossing a reset will automatically be sent in time for the next beam crossing. No deadtime is introduced by events which do not pass Level 1.

The Level 1 calorimeter triggers require that the sum of E_T for all calorimeter towers which are individually over a lower threshold (typically 1 GeV) be greater than a higher threshold (typically 30-40 GeV). Both electromagnetic and hadronic energy, or either one, can be summed in a given tower. The two thresholds are programmable, and four such comparisons are made in a given beam crossing. The results of these comparisons are combined in a trigger "look-up" table with the beam-beam counter coincidence, the muon triggers,[20,24] a stiff track trigger from a fast hardware track processor,[25] and other optional signals to generate the Level 1 decision to accept or reject the event. Different patterns can be rate-limited so that minimum bias events, for example, can be taken intermixed with jet or electron triggers.

The Level 2 trigger starts after a Level 1 trigger has accepted an event. Level 2 uses the same hardware to search the 42 x 24 array of towers in η-ϕ for clusters of total energy or of electromagnetic energy. Towers below a programmable threshold are ignored; a hardware cluster finder identifies clusters of energy in a time of about 200 nsec/cluster. The energies of all towers identified as being in a cluster are summed to form the total E_T and the E_T-weighted first and second η and ϕ moments of the cluster. Separate sums are kept for hadronic and electromagnetic energy. These are digitized and presented as a list of clusters to a fast hardware Level 2 processor. For each cluster a match is made to tracks found in the CTC by the fast (10 μsec) hardware tracking processor, and a coarse

P_T measurement appears in the list if a match is found. Muons are matched to the CTC, and with their momenta also appear in the cluster list.

The final trigger is then a selection on muons, electrons. photons. jets and missing E_T by the programmable Level 2 processor. Many combinations of the above can be programmed in parallel.

Level 3

The Level 3 System is designed to execute FORTRAN-77 filter algorithms as the last stage of on-line trigger selection. Level 3 uses Advanced Computer Program[26] (ACP) 32-bit processors installed in VME crates with VME bus control and interface modules. An interface allows a Fastbus master to transfer data to a processor memory at 20 Mbytes/sec.[27] The processors are double height VME cards based on the Motorola 68020 CPU and 68881 floating point coprocessor. Benchmark studies show the processing capacity of an ACP processor to be about 67% of a VAX 780. For the next run 50 processors will be installed: each processor will have 6 Mbytes of DRAM. Events which pass the Level 3 filter algorithm will be written to tape for off-line analysis.

F. Online Control Systems

The control of the reading of events, detector calibrations, and hardware diagnostics is by a computer process called Run_Control. Subsystems of the detector can be isolated into separate DAQ systems for calibration or diagnosis by multiple copies of Run_Control executing simultaneously on one or several of the VAX processors in the CDF cluster of computers.

During physics data acquisition a single Run_Control process manages the DAQ hardware and the flow of data. Monitoring programs and data diagnostics as well as physics analysis and event selection filters access the data as independent "consumer processes" on either any VAX in the CDF cluster. or remotely via a network. For example, standard processes which access events during data acquisition are programs to identify bad electronics channels, to monitor trigger rates, and to accumulate luminosity information. A separate process ("Alarms and Limits") monitors the status of the detector.

Between data runs calibration processes measure pedestal offsets and gains for the calorimeters, and measure constants for other systems. These data are then stored in large data bases, where they can be extracted at the start of each data run for downloading to the detector subsystems. Other data bases have been created for storing data on external run conditions, integrated luminosity, etc..

which are generated both by the monitoring consumer processes and by the Fermilab Accelerator Control System (ACNET).

G.   Offline Reconstruction of Events

The structure of the offline reconstruction package was determined by the requirement that each physicist from the 17 institutions which constitute the collaboration should be able to do physics with fully corrected data from every CDF subsystem.   Thus the analysis is based on 'parton level' algorithms, available to the whole collaboration, which identify jets, electrons, muons, and neutrinos (by missing E_T), and which incorporate the detailed knowledge of the experts for each subsystem.

Raw data go through a 'production' analysis at Fermilab which generates physics oriented output streams such as jets above several thresholds, multijets, electrons, minimum bias physics, etc., which are written to data summary tapes (DST's).

Before new analysis code is inserted into the libraries it is automatically tested for compatibility with IBM and ACP computers.   The libraries of reconstruction software at computers other than the main Fermilab VAX cluster (including the VAX cluster used by the detector) can be automatically updated by software 'servers,' providing institutions with a current common physics analysis framework.

Acknowledgements

References

1. Each of the systems discussed below is described in detail in Nucl. Instr. and Meth. For even more detail, there exist CDF internal notes on almost all aspects of the detector which can be obtained through the CDF Department, MS 223, Fermilab.

2. The pseudo-rapidity, η, is defined by $\eta \equiv -\ln(\tan \theta/2)$, where θ is the polar angle measured from the proton beam direction. ϕ is the azimuthal angle. CDF uses a conventional right-handed coordinate system with x out of the Tevatron ring in the horizontal plane, y vertical, and z in the proton direction. Forward refers to the proton direction (positive z and η). In the text where the angular coverage of systems is given we use θ_s to measure the angle from either the proton or anti-proton beam, as the detector is forward/backward symmetric.

3. F. Snider et al., Fermilab Pub-87/183-E, submitted to Nucl. Instr. and Meth.

4. M. Atac et al., Fermilab Pub-87/186-E, submitted to Nucl. Instr. and Meth.

5. F. Bedeschi et al., Fermilab Pub-87/182-E, submitted to Nucl. Instr. and Meth.

6. S. Bhadra et al., Fermilab Pub-87/184-E, submitted to Nucl. Instr. and Meth.

7. H. Minemura et al., Nucl. Instr. and Meth. A238, 18 (1985).

8. S. Suzuki et al., Hitachi Densen 1982.12, No. 2, p. 57 (in Japanese).

9. L. Balka et al., Fermilab Pub-87/172-E, submitted to Nucl. Instr. and Meth.

10. Y. Fukui et al., Fermilab Pub-87/173-E, submitted to Nucl. Instr. and Meth.

11. G. Brandenburg et al., Fermilab Pub-87/171-E, submitted to Nucl. Instr. and Meth.

12. S. Bertolucci et al., Fermilab Pub-87/174-E, submitted to Nucl. Instr. and Meth.

13. W. Carithers et al., to be submitted to Nucl. Instr. and Meth.

14. S. Cihangir et al., Fermilab Pub-87/170-E, submitted to Nucl. Instr. and Meth.

15. K. Yasuoka et al., Fermilab Pub-87/175-E, submitted to Nucl. Instr. and Meth.

16. R.G. Wagner et al., Fermilab Pub-87/176-E, submitted to Nucl. Instr. and Meth.

17. S. Hahn et al., Fermilab Pub-87/177-E, submitted to Nucl. Instr. and Meth.

18. T. Devlin et al., Fermilab Pub-87/178-E, submitted to Nucl. Instr. and Meth.

19. G. Ascoli et al., Fermilab Pub-87/179-E and Fermilab Pub-87/180-E, submitted to Nucl. Instr. and Meth.

20. K. Byrum et al., Fermilab Pub-87/181-E, submitted to Nucl. Instr. and Meth.

21. G. Drake et al., Fermilab Pub-87/189-E, submitted to Nucl. Instr. and Meth.

22. E. Barsotti et al., Fermilab Pub-87/190-E, submitted to Nucl. Instr. and Meth.

23. D. Amidei et al., Fermilab Pub-87/187-E, submitted to Nucl. Instr. and Meth.

24. G. Ascoli et al., Fermilab Pub-88/188-E, submitted to Nucl. Instr. and Meth.

25. G.W. Foster et al., Fermilab Pub-87/191-E, submitted to Nucl. Instr. and Meth.

26. H. Areti et al., "The ACP Multiprocessor System at Fermilab," Proceedings of the XXIII International Conference on High Energy Physics, Berkeley, California, July 1986.

27. B. Flaugher et al., "Integration of the ACP Multiprocessor Farm with the CDF FASTBUS Data Acquisition System," Fifth Conference on Real-Time Computer Applications in Nuclear Particle and Plasma Physics, IEEE Transactions on Nuclear Science, NS-34, 865 (1987).

Table Captions

Table 1   A summary of the properties of tracking chambers.

Table 2   The momentum resolution of the detector in different angular regions. θ_s is the polar angle measured relative to either the proton or anti-proton beam.

Table 3   A summary of the calorimeter properties by system.

Table 1

Tracking System	Wire Organization	Inner Layer Coverage	Outer Layer Coverage	Number of (Sense) Wires	Spatial Precision (per hit)	2-Track Resolution
VTPC	8 modules 16 octants/module 24 wires/octant 24 pads/octant	$3.5° < \theta < 176.5°$ $-3.5 < \eta < 3.5$	$8.7° < \theta < 171.3°$ $-2.6 < \eta < 2.6$	3072 wires 3072 pads	200μ-500μ (0-15 cm drift)	$6mm/\theta$ (Z) $6mm$ (r) 3 cm (ϕ)
CTC	9 superlayers 5 axial superlayers of 12 wires each 4 stereo superlayers of 6 wires each	$15° < \theta < 165°$ $-2.0 < \eta < 2.0$	$40° < \theta < 140°$ $-1.0 < \eta < 1.0$	6156	$< 200\mu m$ (r-ϕ) $< 6mm$ (Z)	3.5mm
CDT	3 layers of drift tubes	$40° < \theta < 140°$ $-1.0 < \eta < 1.0$	$40° < \theta < 140°$ $-1.0 < \eta < 1.0$	2016	$200\mu m$ (r-ϕ) $2.5mm$ (Z)	
FTC	one chamber each end 72 cells each 21 wires/cell	$2° < \theta < 10°$ $2.4 < \eta < 4$	$2° < \theta < 10°$ $2.4 < \eta < 4$	3024	$150\mu m$ (r-ϕ)	2mm (ϕ)

Table 2

Angular Region	Tracking Systems	Momentum Resolution: dP_T/p_T^2 $(GeV/c)^{-1}$
$30° < \theta < 150°$	CTC	.002 (no vertex constraint) .001 (100μ beam spot constraint)
$\theta_s = 20°$	CTC	.004 (100μ beam spot constraint)
$\theta_s = 15°$	CTC + VTPC	.035

Table 3

Summary of Calorimeter Properties

	Central		Endwall	Endplug		Forward	
	EM	Hadron	Hadron	EM	Hadron	EM	Hadron
$|\eta|$-coverage	0-1.1	0-0.9	0.7-1.3	1.1-2.4	1.3-2.4	2.2-4.2	2.3-4.2
Tower size, $\Delta\eta \times \Delta\phi$	~0.1×15°	~0.1×15°	~0.1×15°	0.09×5°	0.09×5°	0.1×5°	0.1×5°
Longitudinal samples in tower	1*	1	1	3	1	2	1
Active medium	polystyrene scintillator	acrylic scintillator	acrylic scintillator	Proportional tube chambers with cathode pad readout			
Scintillator thickness or proportional tube size	0.5 cm	1.0 cm	1.0 cm	0.7×0.7 cm^2	1.4×0.8 cm^2	1.0×0.7 cm^2	1.5×1.0 cm^2
Number of layers	31	32	15	34	20	30	27
Absorber	Pb	Fe	Fe	Pb	Fe	94%Pb, 6% Sb	Fe
Absorber thickness	0.32 cm	2.5 cm	5.1 cm	0.27 cm	5.1 cm	0.48 cm	5.1 cm
Typical phototube or wire high voltage	-1100V	-1500V	-1100V	+1700V	+2120V	+1900V	+2200V
Typical phototube or wire gain	1.2×10^5	6×10^5	10^6	2×10^3	2×10^4	5×10^3	10^4
Typical tower signal	-4pC/GeV	-4pC/GeV	-4pC/GeV	+1.25pC/GeV	+1.3pC/GeV	+2pC/GeV	+0.7pC/GeV
Energy (σ/E) resolution at 50 GeV	2%	11%	14%	4%	20%	4%	20%
Typical position resolution at 50 GeV	0.2×0.2 cm^{2*}	10×5 cm^2	10×5 cm^2	0.2×0.2 cm^2	2×2 cm^2	0.2×0.2 cm^2	3×3 cm^2
Characteristic width of azimuthal boundary region	3.5 cm	4.1 cm	3.8 cm, 8.9 cm alternating	0.9 cm	0.8 cm	0.7 cm; 3.2 cm**	1.3 cm; 3.2 cm**

*An imbedded proportional tube chamber at shower maximum gives some additional information. The quoted position resolution is measured with this chamber.

**The first number is for the vertical boundary, the second for the horizontal.

Figure Captions

Figure 1   A perspective view of the CDF detector showing the central detector and the forward and backward detectors.

Figure 2   The CDF Central Detector in its assembly position.

Figure 3   The Central Detector with the calorimeter arches retracted for servicing. The end plugs have been removed, and the central tracking chamber is being installed in the solenoid magnet.

Figure 4   An elevation view of the collision hall and assembly building for the detector.

Figure 5   A cut-away view through the forward half of CDF. The detector is forward-backward symmetric about the interaction point.

Figure 6   A forward muon spectrometer and forward shower counter and hadron calorimeter.

Figure 7   Two of the eight Vertex Time Projection Chamber (VTPC) modules.

Figure 8   An elevation view of the beam pipe and the tracking systems nearest to it. Note that the transverse scale has been magnified.

Figure 9   The amount of material in radiation lengths versus polar angle.

Figure 10   One of the Forward Tracking Chambers (FTC), showing the radial layout of the wires.

Figure 11   An endplate of the Central Tracking Chamber (CTC) showing the arrangement of the blocks which hold the 84 layers of sense wires.

Figure 12   A section of the Central Drift Tube (CDT) system showing the three layers of drift tubes which give a correlated r-ϕ-z measurement for particle tracks. Also shown is the outer superlayer of wires (superlayer 8) of the CTC.

Figure 13   Hadron calorimeter towers in one of eight identical η-ϕ quadrants ($\Delta\phi$ = 90°, $\eta > 0$). The heavy lines indicate module or chamber boundaries. The EM calorimeters have complete ϕ-coverage out to η = 4.2.

Figure 14   Reproducibility of the calibration procedure for four wedges. The arrow indicates the expected shift of +0.22% in the beam/source ratio due to the 30 year half-life of ^{137}Cs. The rms error is 0.6%.

FORWARD MAGNETIZED
STEEL TOROIDS

CENTRAL DETECTOR

BACKWARD ELECTROMAGNETIC
AND HADRONIC CALORIMETERS

LOW BETA QUADS

26.2 meters

FORWARD ELECTROMAGNETIC
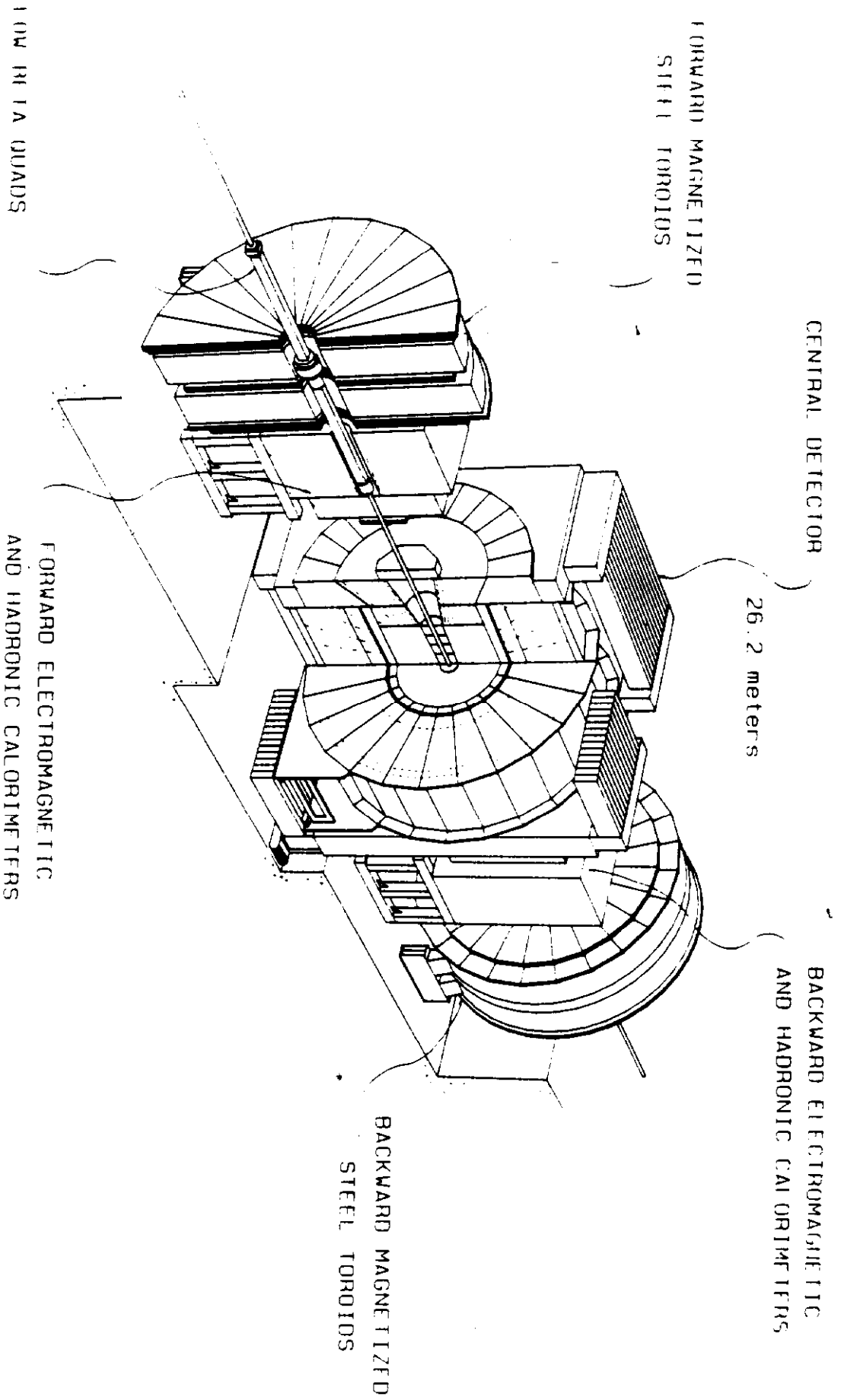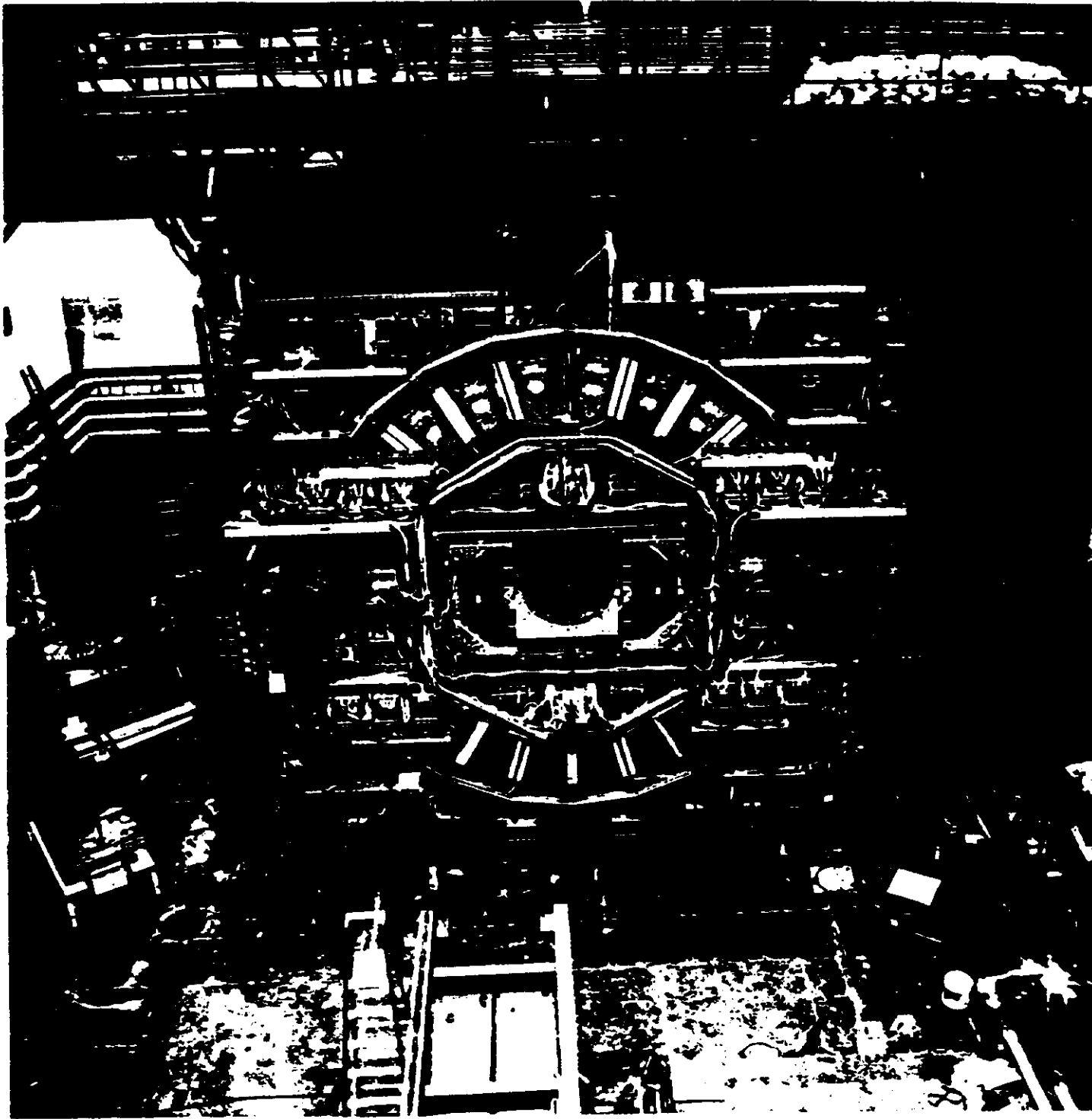AND HADRONIC CALORIMETERS

BACKWARD MAGNETIZED
STEEL TOROIDS

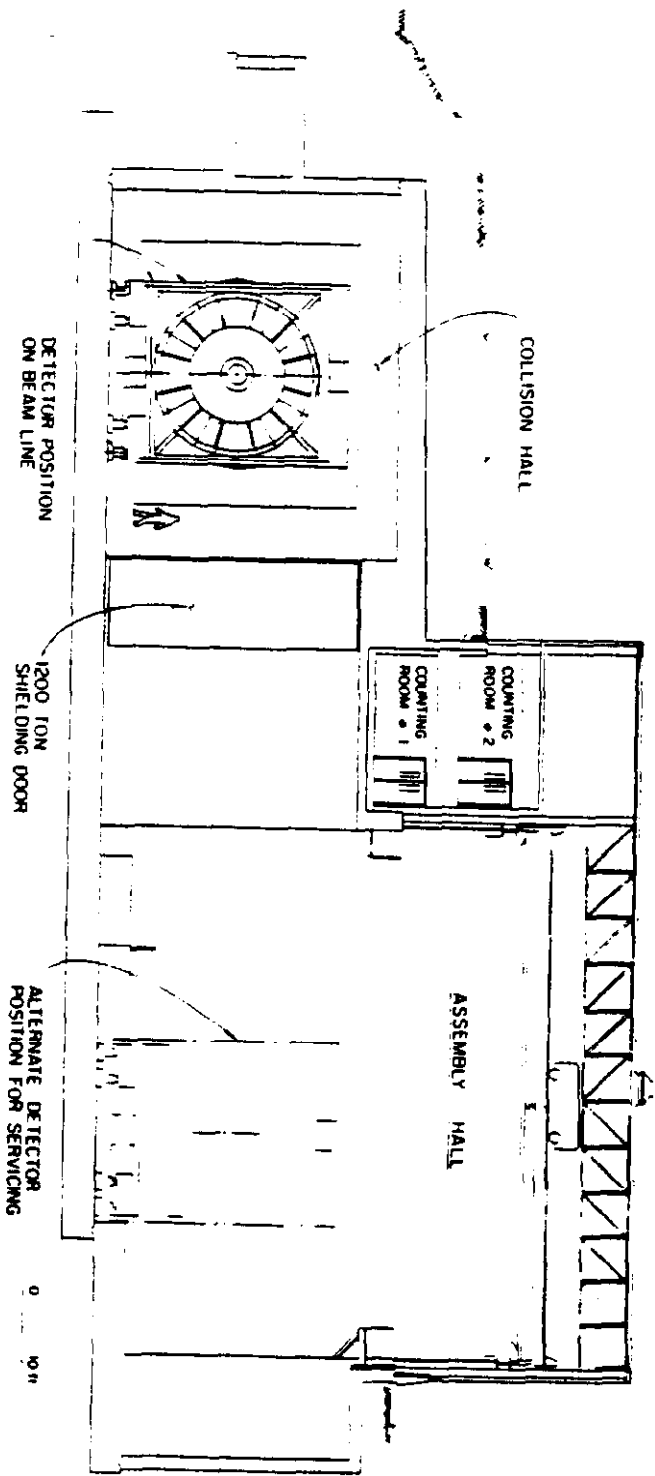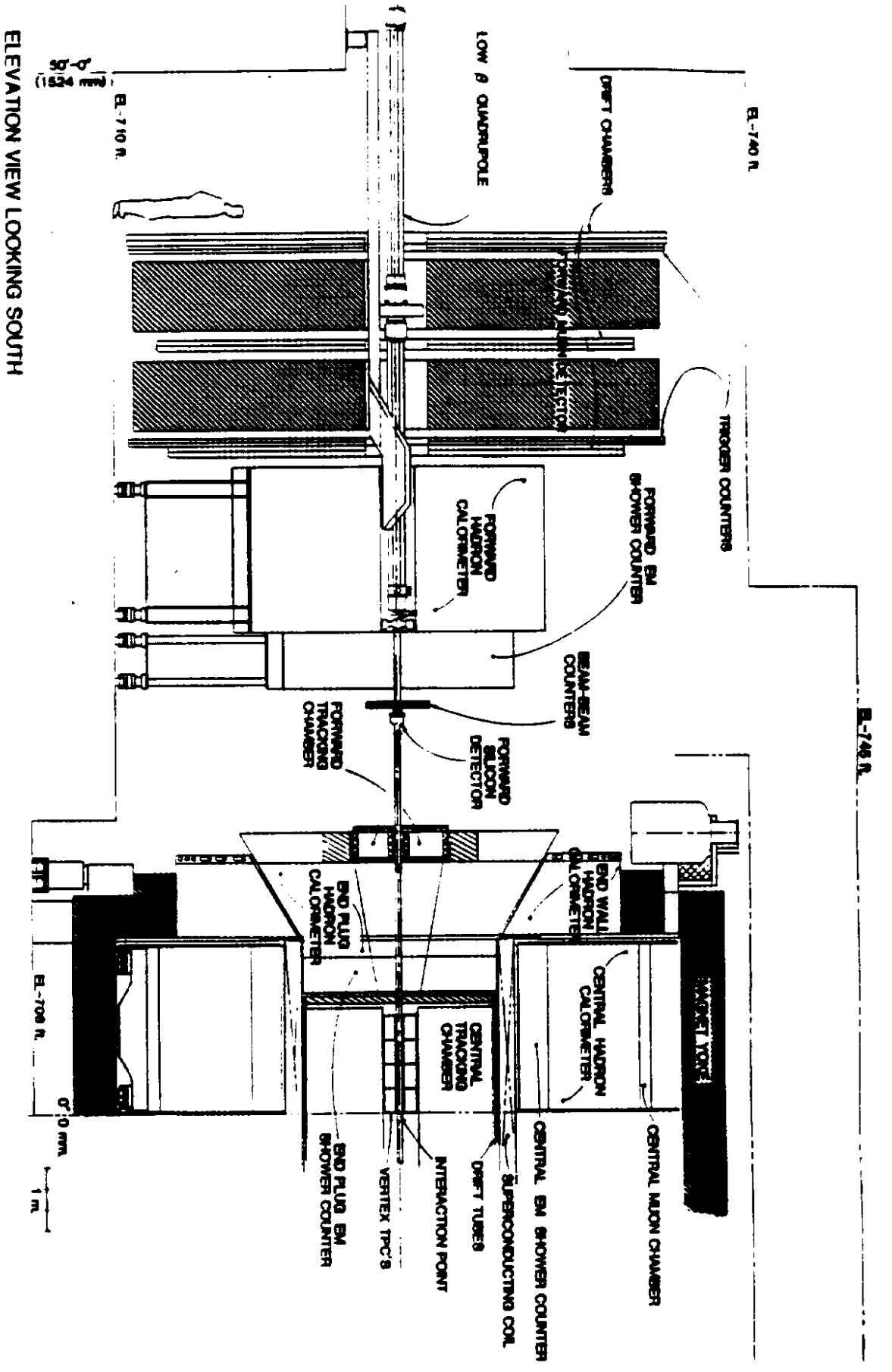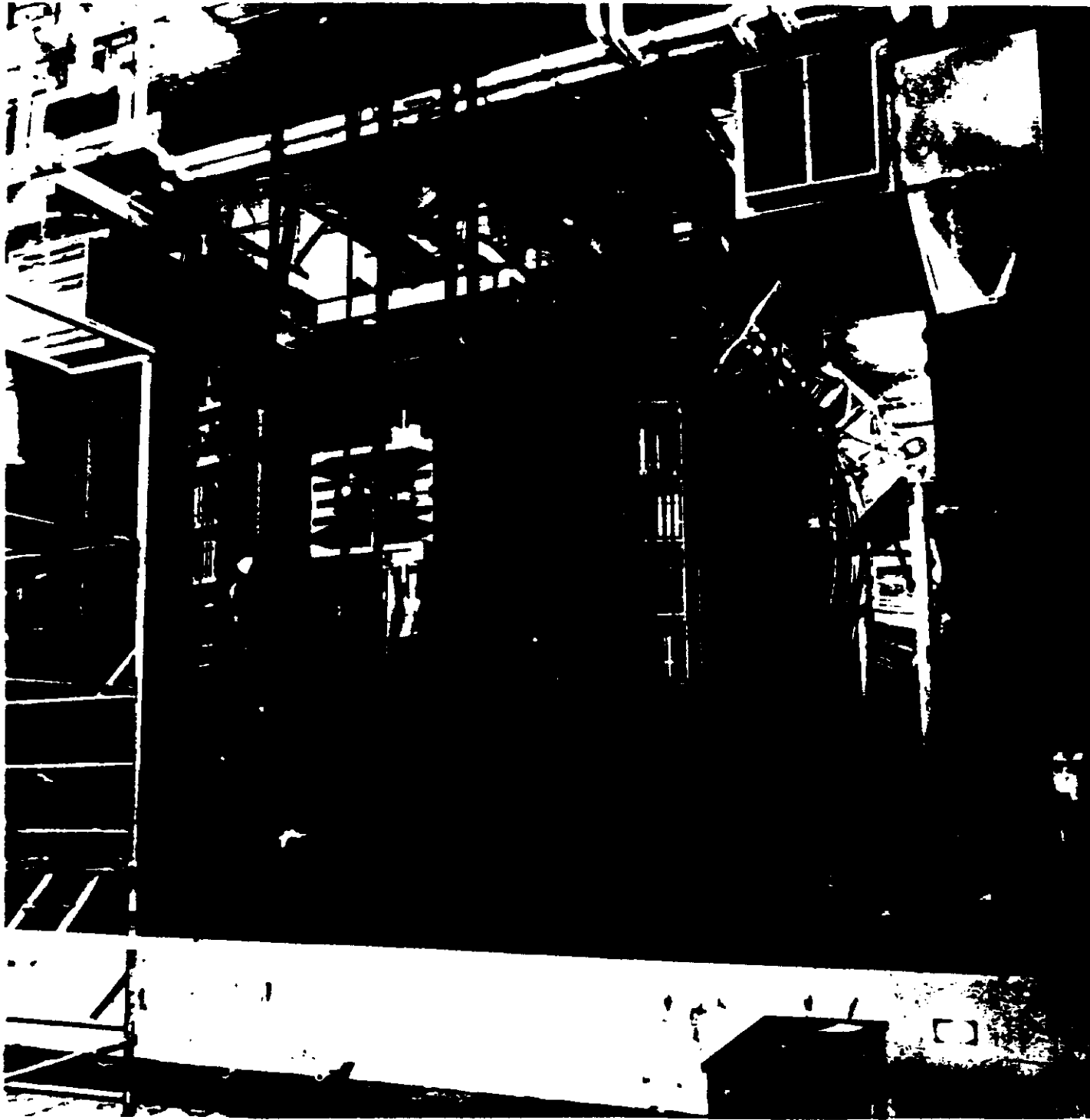Figure 1

CDF-30

CDF-4

Figure 2

CDF—

Figure 3

HORIZONTAL VIEW OF FACILITY

COLLISION HALL

DETECTOR POSITION
ON BEAM LINE

1200 TON
SHIELDING DOOR

COUNTING
ROOM #2

COUNTING
ROOM #1

ASSEMBLY HALL

ALTERNATE DETECTOR
POSITION FOR SERVICING

0 ... 10 ft

Figure 4

ELEVATION VIEW LOOKING SOUTH

Figure 5

CDF-11
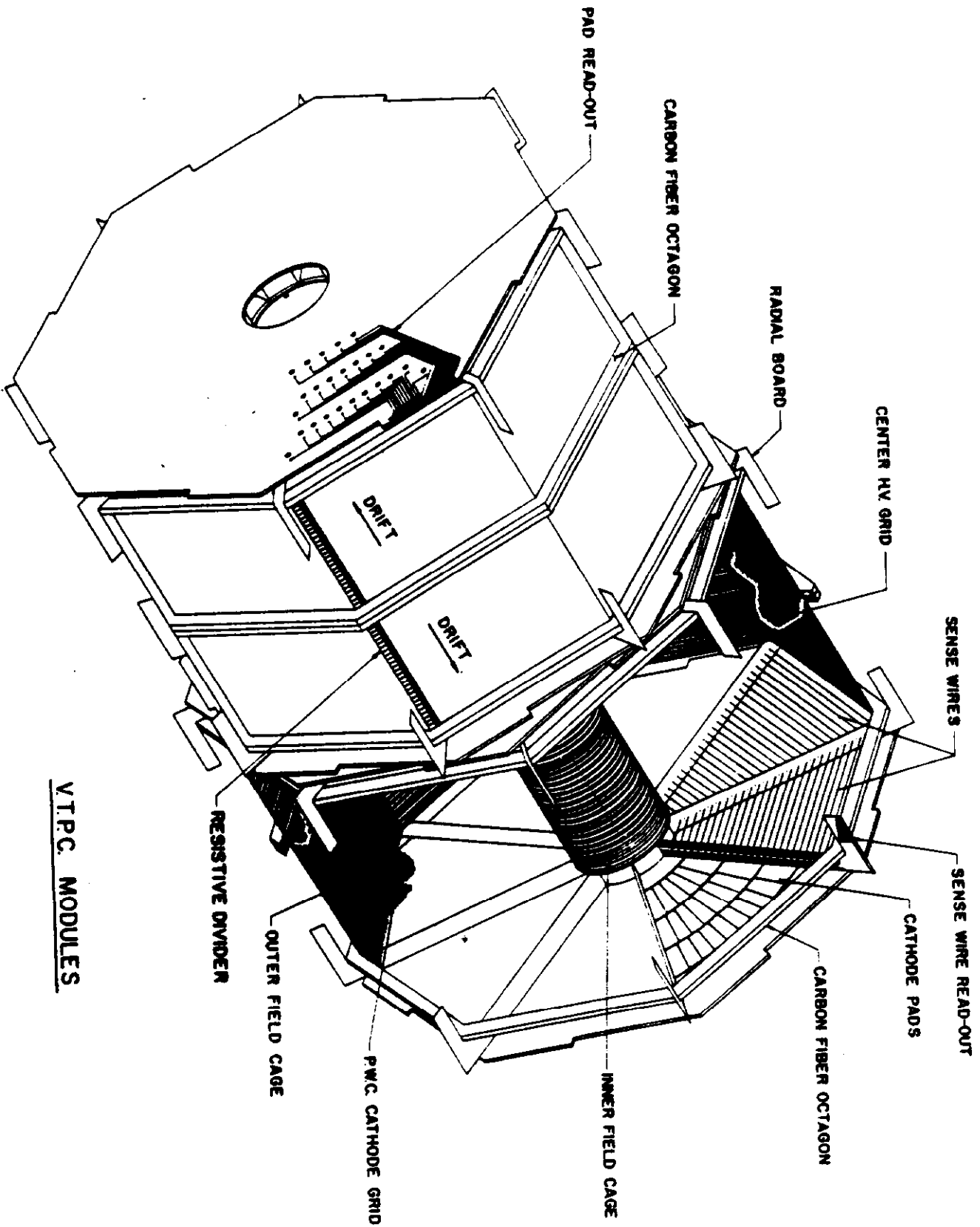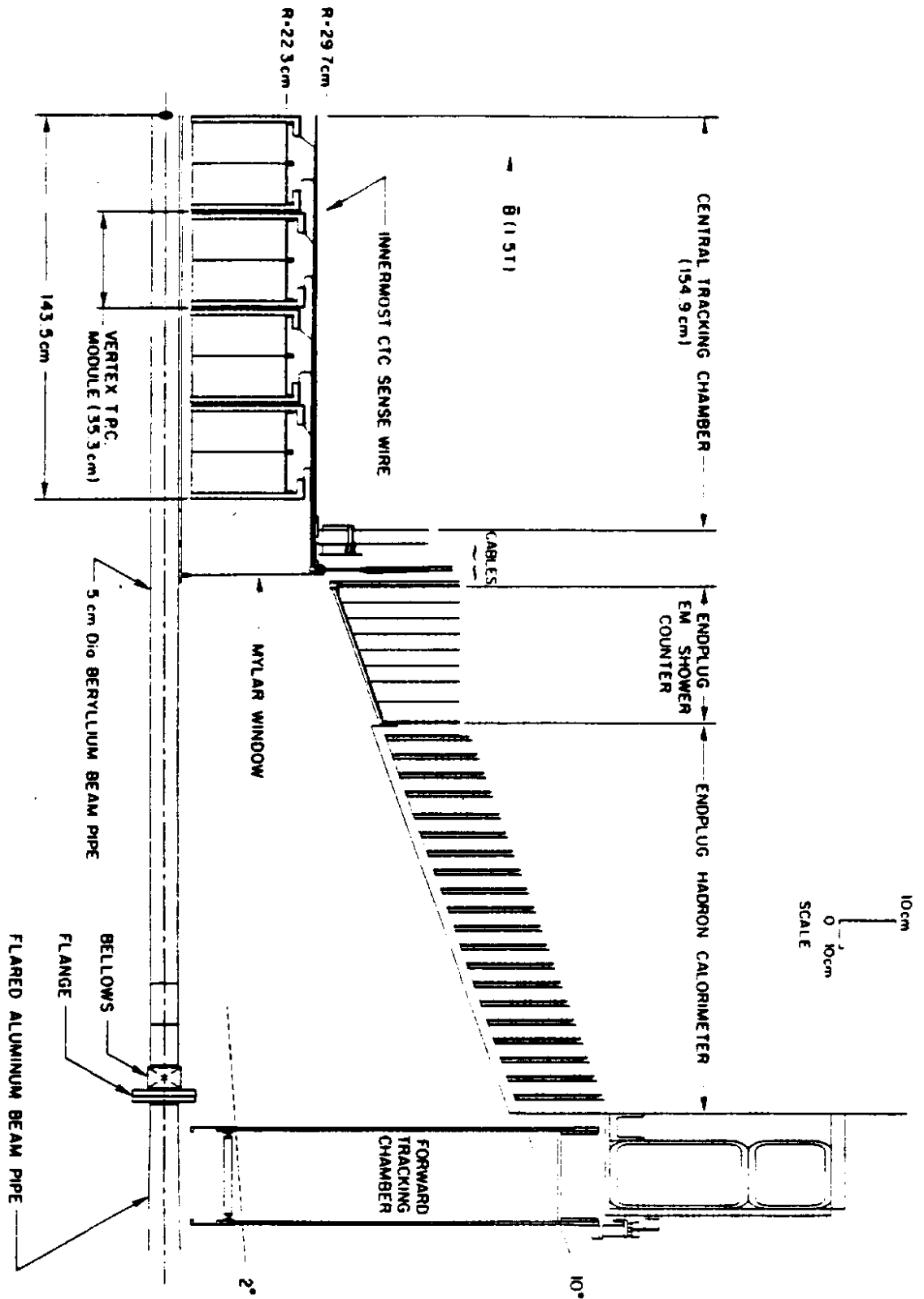
CDF-4

Figure 6

PAD READ-OUT

CARBON FIBER OCTAGON

RADIAL BOARD

CENTER H.V. GRID

SENSE WIRES

SENSE WIRE READ-OUT

CATHODE PADS

CARBON FIBER OCTAGON

INNER FIELD CAGE

PWC. CATHODE GRID

OUTER FIELD CAGE

RESISTIVE DIVIDER

DRIFT

DRIFT

V.T.P.C. MODULES

Figure 7

CDF-12

Figure 8

CDF-32

% RADIATION LENGTH λ VS POLAR ANGLE θ

Figure 9

CDF-33

FORWARD TRACKING CHAMBER

SENSE WIRE PLANE

CATHODE STRIPS

Figure 10

φ

554.00 mm I.D.

2760.00 mm O.D.

Figure 11

CDF-35
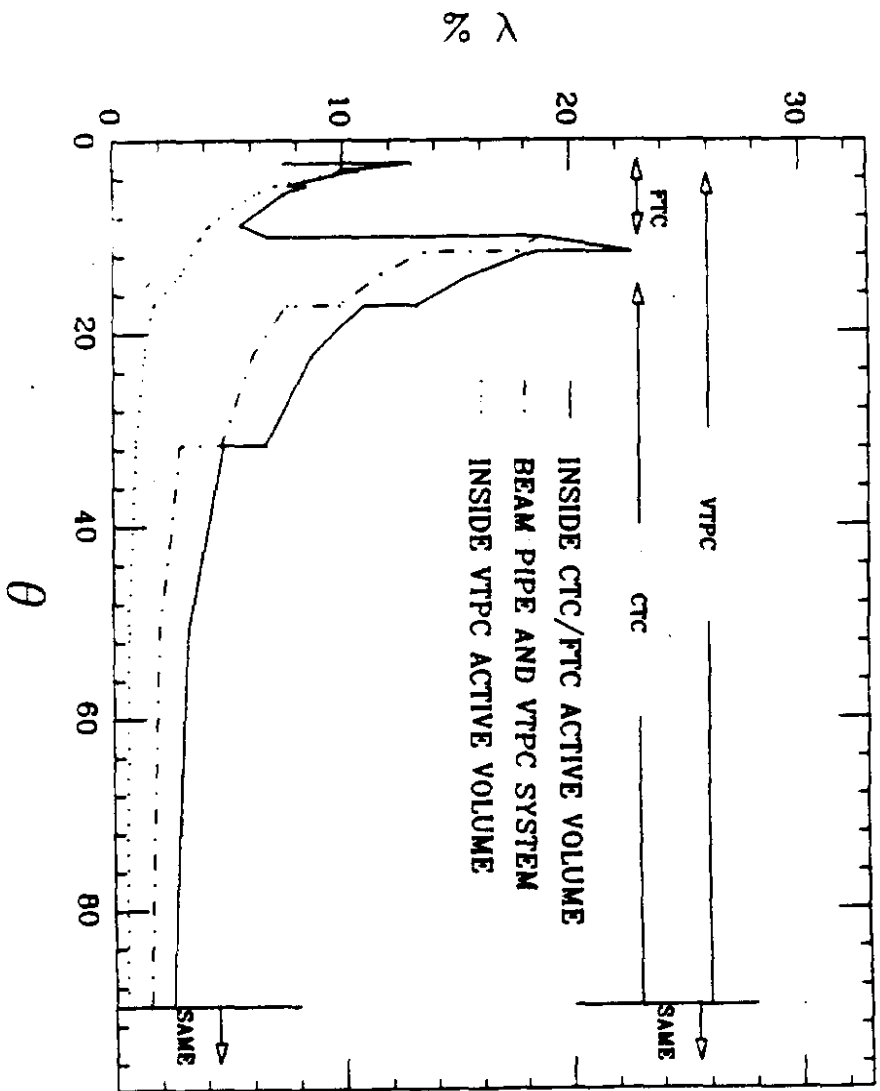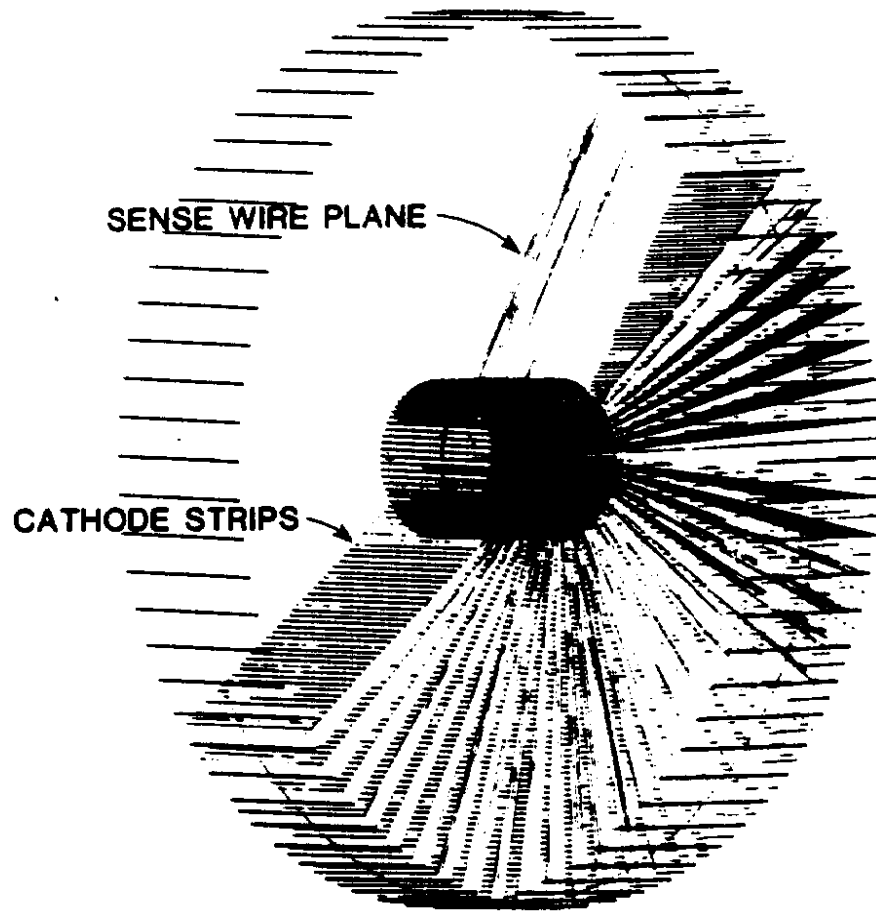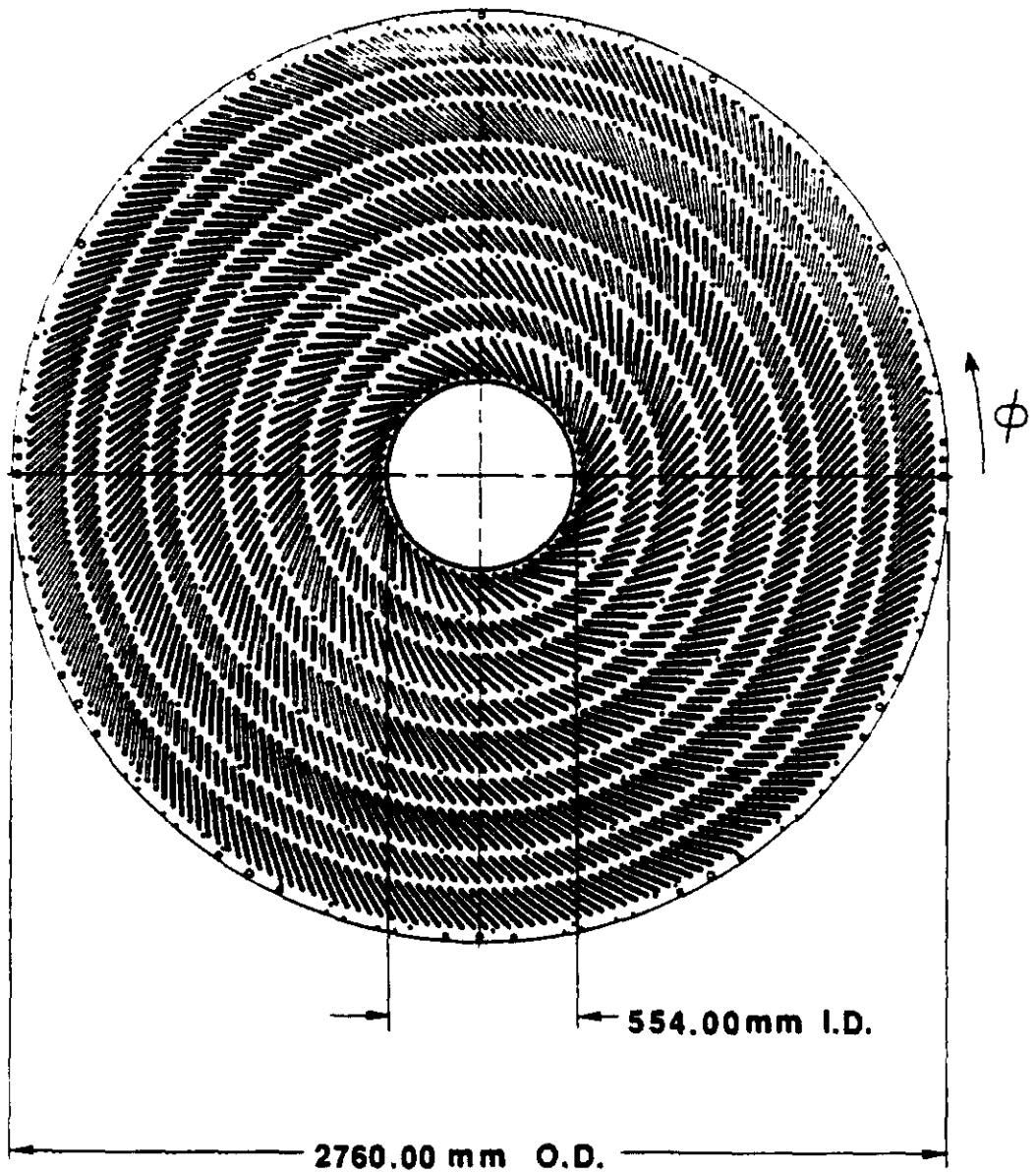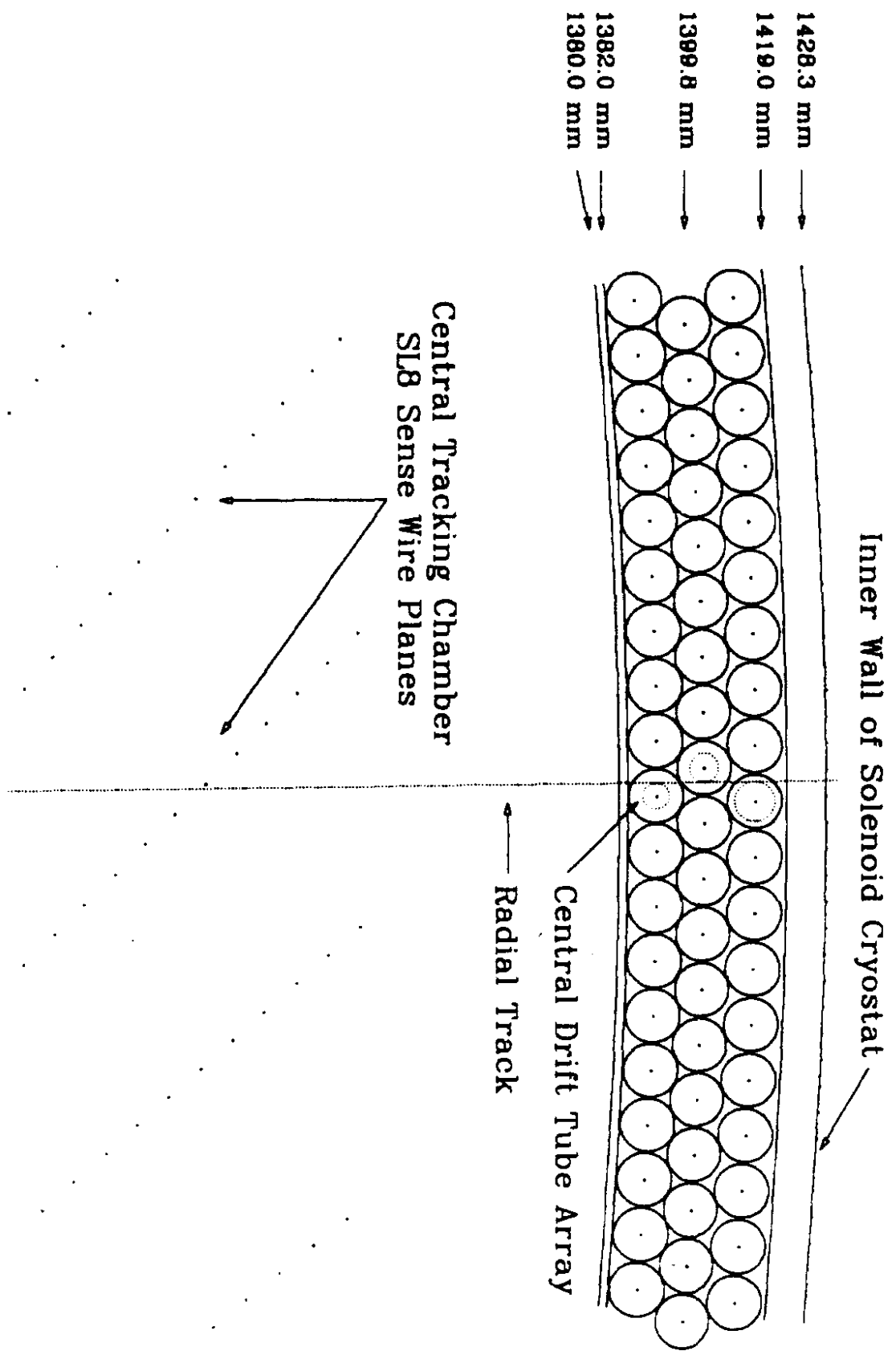
Figure 12. Detail of the CDT array and CTC geometry.

Figure 12

Figure 13

CENTRAL EM CALORIMETER
Calibration Differences

ENTRIES / 0.2 %

$$\left(\frac{Beam}{Source}\right)_{t+\Delta t} - \left(\frac{Beam}{Source}\right)_t \quad \text{for } <\Delta t> = 35\text{days}$$

Wedge 30
Wedge 11
Wedge 1
Wedge 30

Figure 14

CDF−37

Y

X

Y

Z

MUON
CHAMBERS

2260 mm

CENTRAL
CALORIMETER
WEDGE

3470 mm

φ=6.31°

φ=7.50°

θ=88.5°

θ=55.9°

φ

θ

Figure 15

CDF-20

Figure 16

CDF-38

Figure 17

Photomultiplier

Lucite Light Gu

Scintillator

Beam Pipe

0   I meter

Figure 18

Figure 19

ANTIPROTON SPECTROMETER

ELASTIC SCATTERING

PROTON SPECTROMETER

TEVATRON VACUUM PIPE (3" DIAM)